

Tunable Multimode and Narrowband in a Photonic Quasicrystal Waveguide

Qing Hu, Liu-Yang Sun, Di-Hu Xu, Yu Zhou, Ru-Wen Peng*, and Mu Wang

*National Laboratory of Solid State Microstructures and Department of Physics,
 Nanjing University, Nanjing 210093, China*

In this work, we propose a photonic quasicrystal waveguide, which contains a hollow core surrounded by coaxial dielectric quasiperiodic multilayer. Due to the self-similarity in the cladding structure, multiple omnidirectional photonic band gaps (PBGs) exist in the waveguide. The light waves with the frequencies within the omnidirectional PBGs are totally reflected, thereafter, the transport of multimodes is achieved in the quasiperiodic waveguide. Further, it is shown that the centre frequency and the width of the omnidirectional PBG can be tuned by the refractive indexes or the generations of the quasiperiodic sequence in the cladding multilayer. As a consequence, both the quality factor and the confinement performance of the waveguide can be significantly enhanced by decreasing the width of the omnidirectional PBGs. The investigations make it possible to design miniaturized multifunctional optical devices, such as on-chip narrowband waveguide-based filters and laser resonators.

Keywords: Quasicrystal Waveguide, Multimodes, Narrow Bands, High Quality Factor.

1. INTRODUCTION

In the past decades, great efforts have been devoted in controlling light in order to make photons as an alternative carrier for information transfer. Various schemes have been proposed to confine the light. Among them, photonic crystals (PCs)^{1–3} have been extensively studied and exhibit unique capabilities of manipulating and trapping photons. Nowadays, optical devices based on PCs are considered for the applications in integrated photonic circuits. Some PC devices, such as PC cavities,^{4,5} filters,⁶ laser^{7,8} and waveguides⁹ have been investigated so far due to their potential applications in compact, miniaturized and multifunctional optical circuits and all-optical communication networks.

Among various PC devices, PC waveguides are key components for manipulating, confining and guiding light in wavelength-scale microstructure. Generally, there are two kinds of PC waveguides: one is a bunch of rods (or capillaries) positioned in a stack with introducing an extra hole into the center of the pattern by replacing several rods (or capillaries);¹⁰ the other is cylindrical waveguide with a core surrounded by coaxial Bragg mirror multilayer. For decades, PC waveguides have been well investigated both theoretically and experimentally.^{11–13} It has been

demonstrated that the PC waveguides have the excellent performances, such as minimizing effects associated with material nonlinearities and losses and transmitting light around a sharp bent with a small radius of curvature.¹² Recently, it is reported that a PC waveguide surrounded by coaxial self-similar multilayer instead of the Bragg mirror achieves different frequencies guided selectively and separated spatially,¹⁴ which implies that the structure of the PC waveguide can be innovated to achieve novel and unusual properties. In this work, we show that multiple omnidirectional PBGs exist in the photonic quasicrystal waveguide (PQW), which contains a hollow core surrounded by coaxial dielectric quasiperiodic multilayer. The width of these PBGs can be tuned to be extremely narrow by altering the refractive indexes or the generations of the quasiperiodic sequence of the cladding layers. Furthermore, it is found that the ultra-narrow omnidirectional PBGs can also support multimodes in the PQW, and the quality factor and the confinement performance of the modes can be significantly enhanced due to the self-similarity of the PQW.

2. THEORETICAL MODEL

The photonic quasicrystal waveguide (PQW) is designed with a hollow core surrounded by coaxial Thue-Morse multilayer. The Thue-Morse sequence is one of the well-known 1D quasiperiodic structures.^{15,16} The Thue-Morse

*Author to whom correspondence should be addressed.

sequence contains two building blocks *A* and *B*, and is produced by repeating application of the substitution rules $A \rightarrow AB$ and $B \rightarrow BA$. In the PQW (as schematically shown in Fig. 1(a) and its cross section in Fig. 1(b)), the coaxial Thue-Morse multilayer consists of two building blocks *A* and *B* with refractive index n_A and n_B , thickness d_A and d_B , respectively.

In the cylindrical system, the propagation of the electromagnetic wave along the z axis follows the Helmholtz wave equation, which has the form as

$$\nabla^2 \vec{\psi} + k^2 \vec{\psi} = \left(\frac{\partial^2 \vec{\psi}}{\partial r^2} + \frac{1}{r} \frac{\partial \vec{\psi}}{\partial r} + \frac{1}{r^2} \frac{\partial^2 \vec{\psi}}{\partial \theta^2} + \frac{\partial^2 \vec{\psi}}{\partial z^2} \right) + k^2 \vec{\psi} = 0 \quad (1)$$

where $\vec{\psi}$ stands for the components of the electric and magnetic fields, k is the wave vector with the form as $k^2 = \omega^2 \epsilon \mu$ (Here ω is the angular frequency, ϵ and μ are the permittivity and permeability, respectively.) Due to the symmetry of the coaxial multilayer waveguide, we get the axial field components in the i th layer of refractive index n_i with the general form as

$$\Phi(z, r, \theta) = [aJ_m(k_i r) + bY_m(k_i r)] \times (c_1 e^{im\theta} + c_2 e^{-im\theta}) e^{i(\omega t - k_z z)} \quad (2)$$

where Φ stands for either E_z or H_z ; $J_m(x)$ and $Y_m(x)$ are Bessel functions of the first and second kind, respectively; and k_i is the transverse wave vector $k_i = \sqrt{(n_i \omega/c)^2 - k_z^2}$ (Here k_z is the propagation wave vector). From E_z and H_z , the corresponding radial and angular components of the electromagnetic field E_r , E_θ , H_r , H_θ can be calculated. Based on the transfer matrix method, the electric and magnetic components in the $(i+1)$ th layer can be derived by those in the adjacent i th layer of the waveguide. Obviously, the transfer matrix depends on the photonic frequencies, the propagation wave vector, and the geometry of the dielectric cladding layers.

By using the transfer matrix method and Bloch theorem,^{14, 17–18} the photonic band structure for the transverse electric (TE) and transverse magnetic (TM) polarization modes can be calculated. In order to specify the PBGs in the waveguide, we use two theoretical quantities: the width

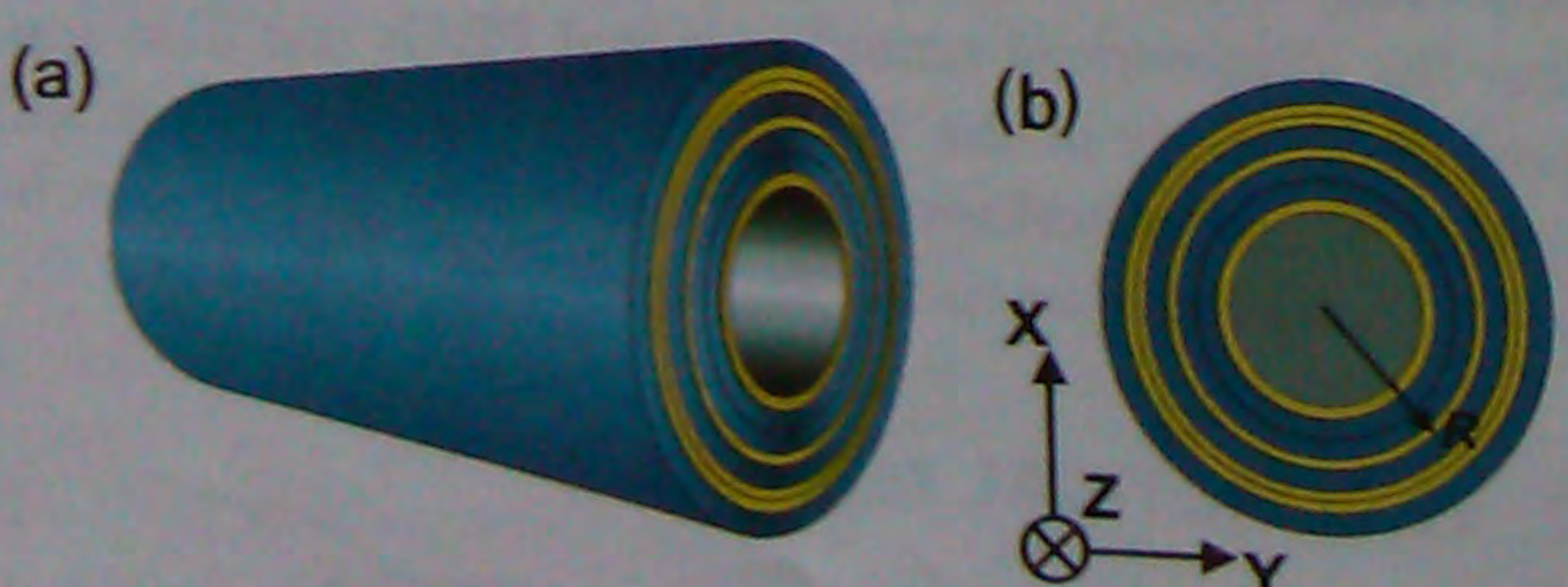


Fig. 1. The schematic PQW (a) and its cross section (b). In the PQW, a hollow core (refractive index $n_0 = 1$) of a radius R_0 is surrounded with a coaxial Thue-Morse multilayer consisting of two building blocks *A* (yellow) and *B* (blue).

and the centre frequency of the omnidirectional PBGs.¹⁹ Here, the width of the omnidirectional PBG is defined as

$$\delta\omega = \omega_h - \omega_l \quad (3)$$

where ω_h is the band edge of the grazing incidence (perpendicular to the axial direction), which corresponds to $k_z = 0$; and ω_l is the edge of the intersection of the top of the TM (TE) allowed band with the light line, which corresponds to $k_z = \omega/c$. And the centre frequency is defined as

$$\omega_c = (\omega_h + \omega_l)/2 \quad (4)$$

It is evident that the centre frequencies and the widths of omnidirectional PBGs depend on the frequency (ω) and the wave vector (k_z) of the light wave, and the structural parameters of the waveguide.

In the following calculations, the radius of the hollow core is set as $R_0 = 3a$, the thicknesses as $d_A = 0.33a$ and $d_B = 0.67a$, respectively, and their refractive indexes n_A and n_B are variable. Here a is the characterized size of the PQW, which corresponds to the operating wavelength of the waveguide. In the structure, we set $a = 100$ nm to make the waveguide operate at optical frequency.

3. RESULTS AND DISCUSSION

Figure 2 illustrates the photonic band structure of the PQW, which contains the cladding Thue-Morse dielectric multilayers with different generations S_n (Note: $n = 2$ for the periodic Bragg waveguide). The multilayers have the refractive indexes as $n_A = 2.9$ and $n_B = 1.8$, respectively. As shown in Figures 2(a)–(d), there exist several frequency regions (shown in blue), where the incident plane waves transmit throughout the cladding layers and yet cannot be confined in the PQW; while there also exist the frequency regions (shown in white), where the electromagnetic waves can be confined in the PQW, known as the photonic band gaps (PBGs). The orange areas indicate the frequency regions in which the electromagnetic waves are totally reflected, known as the omnidirectional PBGs. Note that these PBGs are for both transverse electric (TE) and transverse magnetic (TM) polarizations. Comparing with the periodic waveguide (as shown in Fig. 2(a)), in the PQW there are more PBGs at the same frequency range. For example, in the frequency range of $\omega/\omega_0 = 0\sim 0.3$ (Here $\omega_0 = 2\pi c/a$), one PBG exists in the periodic waveguide, while in the PQW with generations S_3 (as shown in Fig. 2(b)) two PBGs exist, and with generations S_5 (as shown in Fig. 2(d)) totally 5 PBGs can be identified. Furthermore, by increasing the generations of PQW, more PBGs occur at the same frequency region (as shown in Figs. 2(c), (d)). These features originate from the quasi-periodic Thue-Morse structure in the waveguide. Actually, due to the self-similarity in the structure, the PBGs in the PQW are furcated. Therefore, the PBGs in the PQW indeed

Fig. 2. The tunable cladding generations S_n : (a) is for periodic both TE and TM pairs for which diagonal black in orange corresponds to radius as $R =$ respectively.

possess the in controlling

In order structure on cies and the national PBG and (4). As ω declines grows. For centre frequ

0.097 ω_0 (at

Fig. 3. Centre and its width with different. Here $n_A = 2.4$ and $n_B = 1.8$ respectively. The narrow corresponding centre indexes $n_A = 2.4$ and $n_B = 1.8$.

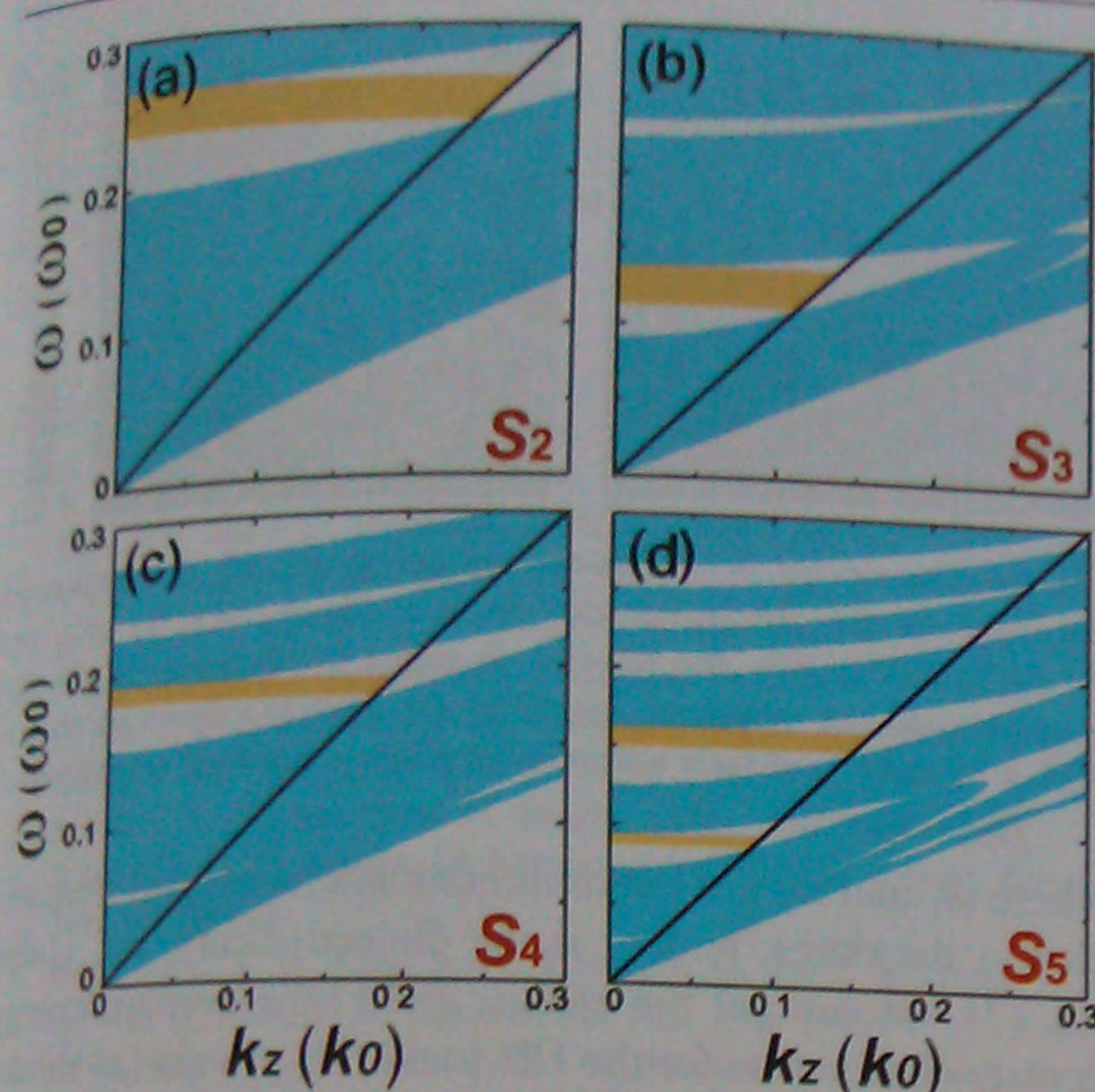


Fig. 2. The calculated photonic band structure of the PQW, which contains the cladding Thue-Morse dielectric multilayer with different generations S_n : (a) S_2 ; (b) S_3 ; (c) S_4 and (d) S_5 , respectively. Among them, S_2 is for periodic photonic crystal waveguide. Note that the PBGs are for both TE and TM polarizations. The blue regions correspond to (k_z, ω) pairs for which light can propagate through the cladding multilayer. The diagonal black line represents the light line $\omega = ck_z$. The regions shown in orange correspond to the omnidirectional PBGs. The waveguide has a radius as $R = 3.0a$ and the refractive indexes as $n_A = 2.9$ and $n_B = 1.8$, respectively.

possess the furcation feature, which creates the possibility in controlling the propagating modes in the waveguide.

In order to observe the influence of the quasiperiodic structure on the PBGs, we calculate the centre frequencies and the widths of the lowest-frequency omnidirectional PBG as a function of n_A/n_B , by using Eqs. (3) and (4). As shown in Figure 3(a), the centre frequency ω declines from visible range to infrared range as n_A/n_B grows. For example, in the PQW with S_4 ($n_B = 2.0$), the centre frequency drops from $0.17\omega_0$ (at $n_A/n_B = 1.5$) to $0.097\omega_0$ (at $n_A/n_B = 3.5$), corresponding to the wavelength

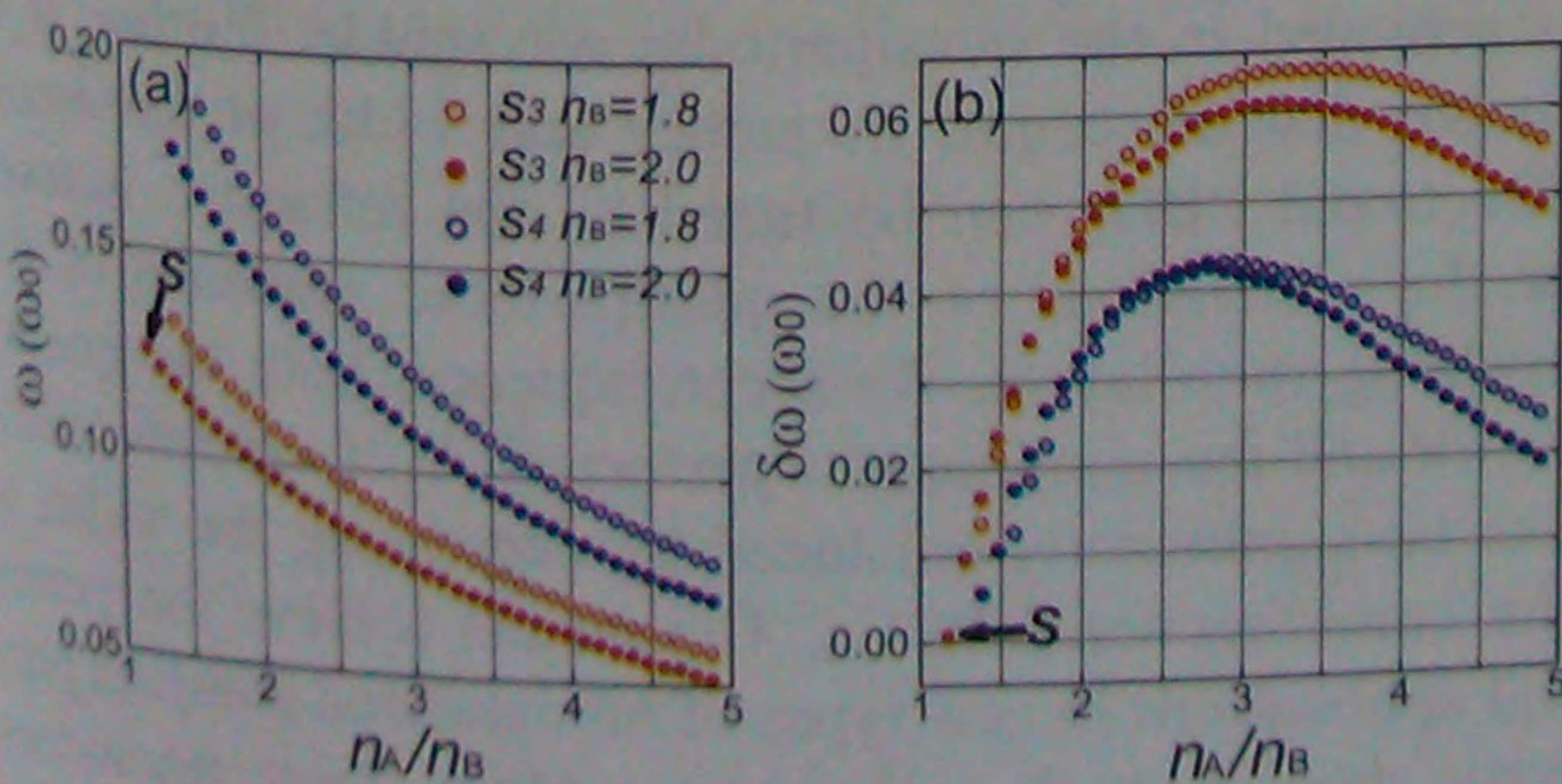


Fig. 3. Centre frequency of the lowest-frequency omnidirectional PBG (a) and its width (b) as a function of the ratio of refractive index n_A to n_B with different generations S_3 (shown in red) and S_4 (shown in blue), respectively. Here n_B has fixed values as 1.8 (hollow circle) and 2.0 (solid circle). The narrowest width of the omnidirectional PBG and its corresponding centre frequency are indicated by arrows, with the refractive indexes $n_A = 2.4$ and $n_B = 2.0$, respectively.

range from 1031 nm to 588 nm. The falling of the centre frequency reveals that the PBGs furcation becomes more obvious when the contrast of refractive indexes enlarges. As shown in Figure 3(b), the width of the omnidirectional PBG $\delta\omega$ has a maximum (nearly at $n_A/n_B = 3$), and turns to be narrower when n_A/n_B becomes larger or smaller. For example, in the PQW with S_3 , the maximum and the minimum widths of the omnidirectional PBG are $0.0613\omega_0$ (at $n_A/n_B = 3.2$) and $0.001\omega_0$ (at $n_A/n_B = 1.2$), respectively, corresponding to the wavelength of 1330 nm and 7 nm. The widely tunable-width omnidirectional PBG in the PQW creates potential applications in kinds of optical devices. Besides, it can be seen that both the centre frequency and width of the omnidirectional PBG in the waveguide with fewer generations are smaller than that with larger ones. That is because of the furcation features of the PBGs in the PQW. The data in Figure 3 provide a basis of devising PQW which possesses different performances such as board band resonator or narrow band filter.

The propagating modes in the PQW can also be obtained by transfer matrix method. Here, we intentionally take the following PQW as an example. The refractive indexes of this waveguide are set as $n_A = 2.0$ and $n_B = 2.0$, respectively, which are indicated by the arrow in Figure 3. In the PQW, there are only two modes in the lowest-frequency omnidirectional PBG (as shown in Fig. 4(a)): HE_{11} and HE_{21} modes, which belong to the TE-like hybrid modes HE_{ml} . Here the label m indicates the angular momentum ($m = 1, 2, \dots$). Note that $m = 0$ corresponds to a pure TE (TM) polarization mode while $m \neq 0$ corresponds to a mixture of TE and TM modes. The HE_{ml} modes have totally six field components: $E_z, E_\theta, E_r, H_z, H_\theta, H_r$. These propagating modes present some features. On one hand, the different types of propagating modes exist in the same PBG (with the frequency range as $\omega/\omega_0 = 0.11$ – 0.13). The frequency ranges of different

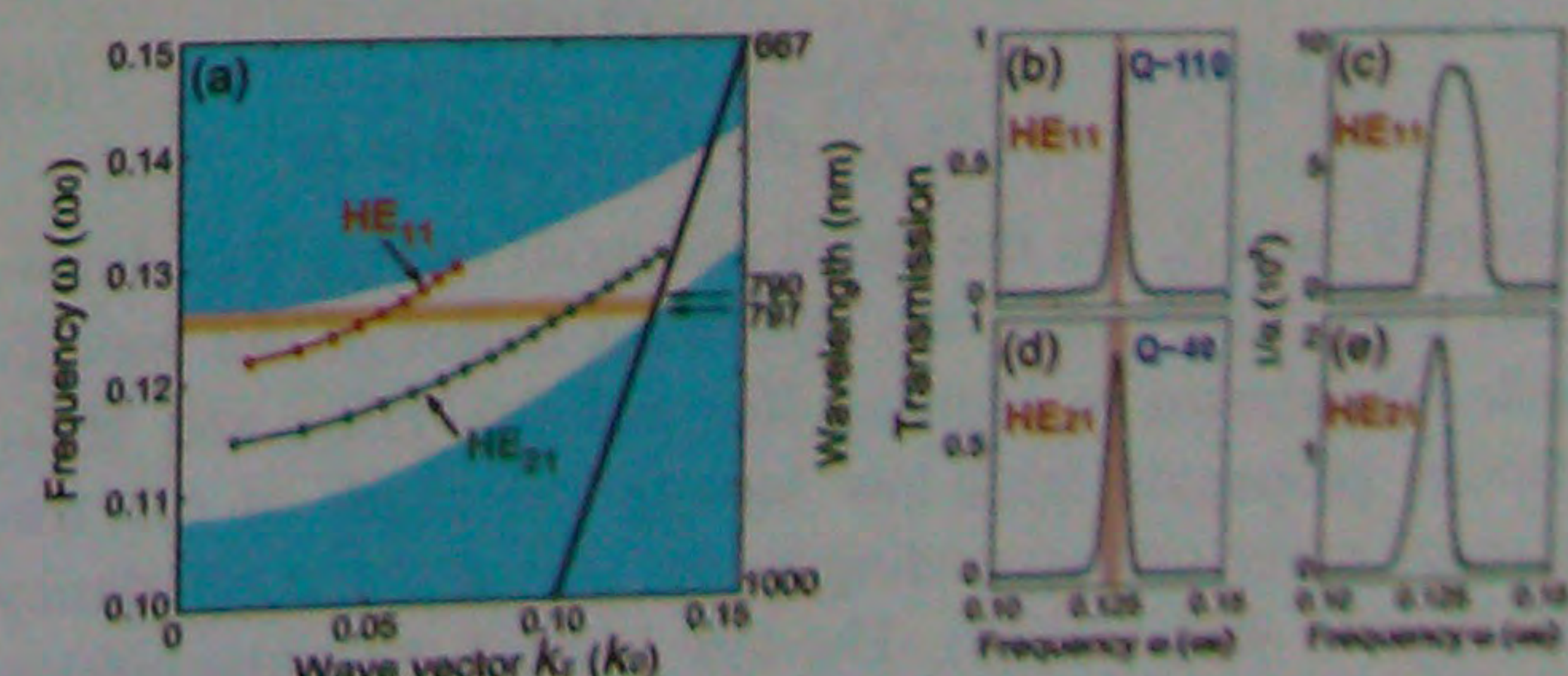


Fig. 4. (a) The transmission modes in PQW with the structural parameters indicated by arrow in Figure 3. The orange region corresponds to the omnidirectional PBG in the waveguide. The calculating modes are shown in circle-line: the red is for HE_{11} , and the green is for HE_{21} . The solid black line is for incident light line. The transmission efficiency as a function of frequency for modes: (b) HE_{11} and (d) HE_{21} , respectively. The pink regions indicate FWHM of the transmission efficiency curves. The reciprocal of the attenuation ($1/\alpha$) as a function of frequency for modes: (c) HE_{11} and (e) HE_{21} , respectively.

modes overlap, implying that the PQW can be used as a multimode waveguide. On the other hand, either type of propagating modes is restricted within the frequency range of the PBG, implying that the transmission frequencies of the modes can be controlled by the PBGs. These features open a way to achieve tunable transmission multibands in waveguide.

In order to evaluate the confinement feature of the PQW, we study the transmission efficiency of light wave in the waveguide. The transmission efficiency (T) in the waveguide is defined as the ratio of the output power of the mode to its total input power, i.e.,

$$T = \frac{\int_0^l l dl \int_0^{2\pi} d\phi \int_0^R (S_{z1} + S_{r1} + S_{\theta1}) r dr}{S_{z0} + S_{r0} + S_{\theta0}} \quad (5)$$

Here S_{z1} , S_{r1} , $S_{\theta1}$ are the axial, radial and azimuthal energy flux densities in the waveguide, and S_{z0} , S_{r0} , $S_{\theta0}$ are the initially incident axial, radial and azimuthal energy flux densities, respectively; R is the outermost radius and l is the unit length (1 cm). For the modes HE_{11} and HE_{21} , we calculate their transmission efficiency as a function of frequency (as shown in Figs. 4(b) and (d)). It is obvious that both curves have the transmission peaks at the same frequency, which correspond to the centre frequency of the omnidirectional PBG marked by the arrow in Figure 3(a). Furthermore, the transmission efficiency is large in the omnidirectional PBG while sharply declines outside that. The quality factors of the PQW are calculated as 110 for HE_{11} mode and 40 for HE_{21} mode, respectively. Note that although the quality factor of the PQW is not as high as that of a photonic crystal,²⁰ the FWHM of the transmission efficiency (shown in pink in Figs. 4(b) and (d), with the value as 7 nm) is comparable with the bandwidth of a band-pass filter based on PCF.²¹

The attenuation of the mode (α) in the waveguide is also calculated to quantify the transmission performance of the waveguide. Here we take the definition presented in Ref. [14] as the ratio of the radially-outgoing power of the mode to its forward-propagating power in the waveguide.

$$\alpha(\omega) = \frac{S_r |_{r=R} \times (2\pi R l)}{\int_0^l l dz \int_0^{2\pi} d\phi \int_0^R S_z(r, \phi) r dr} \quad (6)$$

where S_r and S_z are the radial and axial energy flux densities, respectively; R is the outermost radius of the waveguide. As shown in Figures 4(c) and (e), HE_{11} and HE_{21} modes propagate with low loss in the PQW at the frequency range corresponding to the transmission efficiency in Figures 4(b) and (d). The low loss of the transmission modes demonstrates the well confinement performance of the PQW.

In the following, we investigate the electric-field distribution of the transmission modes in the PQW. The time-average electric-field energy density in the frequency range ($\omega_2 - \omega_1$) in the PQW can be summed as

$$\Gamma = \frac{1}{2} \int_{\omega_1}^{\omega_2} \epsilon_r (|\vec{E}(\omega)|)^2 d\omega \quad (7)$$

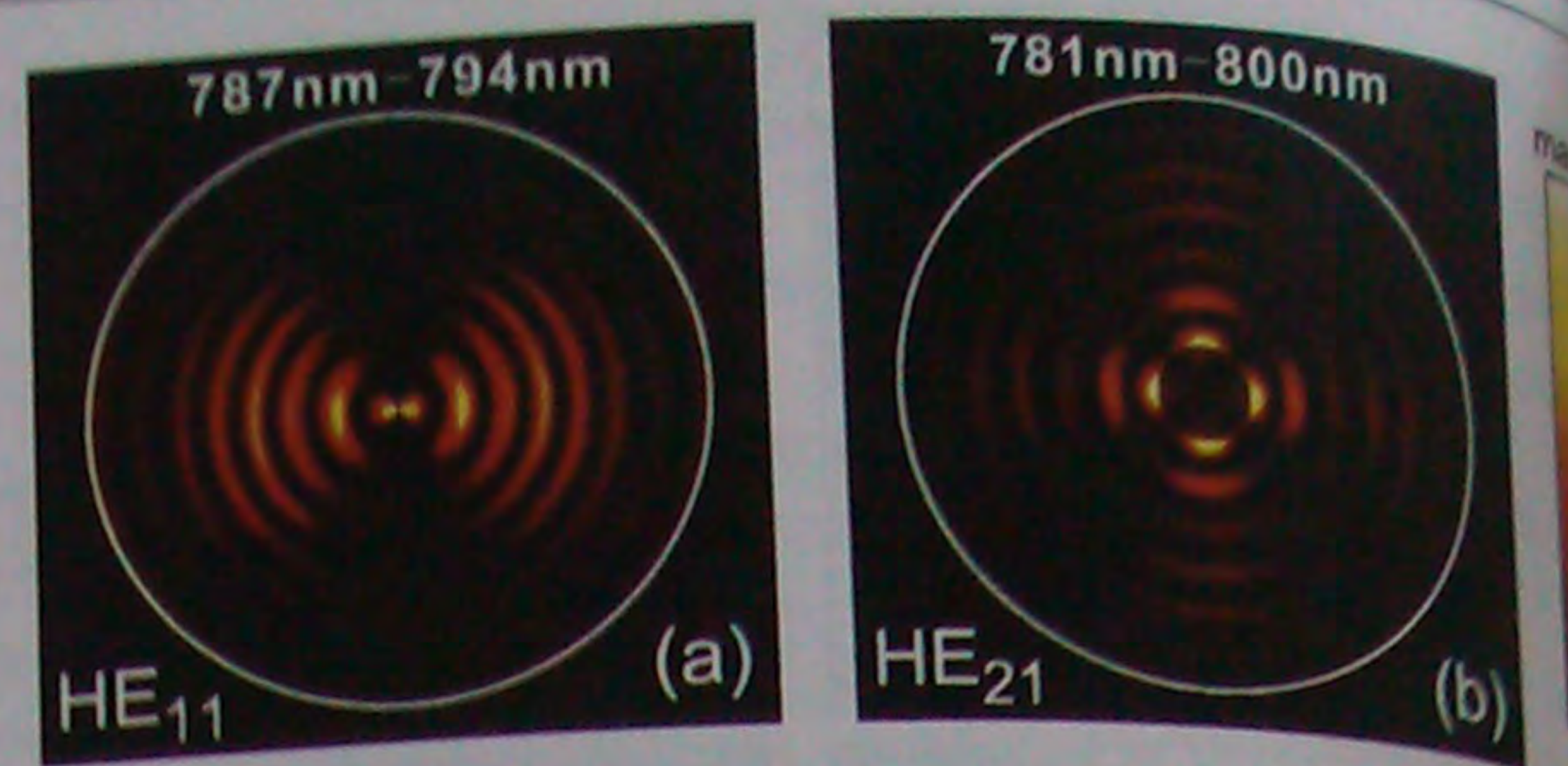


Fig. 5. The electric-field time-average energy density distributions in the PQW for the different modes given in Figure 4(a): (a) HE_{11} and (b) HE_{21} , respectively. The wavelength ranges of HE_{11} and HE_{21} modes correspond to the frequency ranges of the FWHM (shown in pink in Figs. 4(b) and (c)) of their transmission efficiency curves, respectively.

where ω_1 and ω_2 are the minimum and maximum frequencies in the range, and ϵ_r is the dielectric constant. Using Eq. (7), we can get the electric-field time-average energy density distribution for the HE_{11} and HE_{21} mode (as shown in Fig. 5) at the frequency range corresponding to the FWHM of the transmission efficiency. It is obvious that the two modes are both well confined in the PQW with the wavelength range of 787 nm–794 nm for HE_{11} (Fig. 5(a)) and 781 nm–800 nm for HE_{21} (Fig. 5(b)), respectively. Furthermore, the patterns of the modes are different, which are dipole-like for HE_{11} , and quadrupole-like for HE_{21} , respectively. Such difference originates from the different angular momentum m of the modes ($m = 1$ for HE_{11} and $m = 2$ for HE_{21} , respectively).

4. CONCLUSIONS

We have investigated the omnidirectional PBGs and the transmission performances in the photonic quasicrystal waveguide, which contains a hollow core surrounded by coaxial dielectric quasi-periodic multilayer. Due to the self-similarity in the cladding structure, multiple omnidirectional PBGs exist in the waveguide. The light waves with the frequencies within the omnidirectional PBGs are totally reflected, thereafter, the propagation of multimodes is achieved in the quasiperiodic waveguide. Further, it is shown that the centre frequency and width of the omnidirectional PBGs can be tuned by the refractive indexes or the generations of the quasiperiodic sequence in the cladding multilayers. As a consequence, both the quality factor and the confinement performance of the waveguide can be significantly enhanced by decreasing the width of the omnidirectional PBGs. The results achieve the potential applications in new types of miniaturized compact photonic devices, such as band-pass filters, laser resonators and narrow band fiber cavities.

Acknowledgments: This work was supported by the State Key Program for Basic Research from the Ministry of Science and Technology of China (Grants Nos. 2012CB921502, and 2010CB630705), the National

Natural Science Foundation of China (Grant Nos. 11034005, 61077023, 50972057, and 11021403), and partly by Jiangsu Province (Grant No. BK2008012, PAPD) and Ministry of Education of China (Grant No. 20100091110029).

References and Notes

1. E. Yablonovitch, T. J. Gmitter, R. D. Meade, A. M. Rappe, K. D. Brommer, and J. D. Joannopoulos, *Phys. Rev. Lett.* **67**, 3380 (1991).
2. J. Zi, J. Wan, and C. Zhang, *Appl. Phys. Lett.* **73**, 2084 (1998).
3. Z. Y. Li, B. Y. Gu, and G. Z. Yang, *Phys. Rev. Lett.* **81**, 2574 (2007).
4. J. S. Foresi, P. R. Villeneuve, J. Ferrera, E. R. Thoen, G. Steinmeyer, S. Fan, J. D. Joannopoulos, L. C. Kimerling, H. I. Smith, and E. P. Ippen, *Nature* **390**, 13 (1997).
5. S. Noda, A. Chutinan, and M. Imada, *Nature* **407**, 608 (2000).
6. F. Benabid, J. C. Knight, G. Antonopoulos, P. S. J. Russell, *Science* **298**, 399 (2002).
7. H. G. Park, S. H. Kim, S. H. Kwon, Y. G. Ju, J. K. Yang, J. H. Baek, S. B. Kim, Y. H. Lee, *Science* **305**, 1444 (2004).
8. Y. Chassagneux, R. Colombelli, W. Maineult, S. Barbieri, H. E. Beere, D. A. Ritchie, S. P. Khanna, E. H. Linfield, and A. G. Davies, *Nature* **457**, 174 (2009).
9. J. S. Skibina, R. Iliew, J. Bethge, M. Bock, D. Fischer, V. I. Beloglasov, R. Wedell, and G. Steinmeyer, *Nature Photonics* **2**, 679 (2008).
10. P. Russell, *Science* **299**, 358 (2003).
11. J. C. Knight, J. Broeng, T. A. Biks, P. St, and J. Russell, *Science* **282**, 1476 (1998).
12. M. Ibanescu, Y. Fink, S. Fan, E. L. Thomas, and J. D. Joannopoulos, *Science* **289**, 415 (2000).
13. B. Temelkuran, S. D. Hart, G. Benoit, J. D. Joannopoulos, and Y. Fink, *Nature* **420**, 650 (2002).
14. Q. Hu, J. Z. Zhao, R. W. Peng, F. Gao, R. L. Zhang, and M. Wang, *Appl. Phys. Lett.* **96**, 161101 (2010).
15. F. Qiu, R. W. Peng, X. Q. Huang, X. F. Hu, Mu Wang, A. Hu, S. S. Jiang, and D. Feng, *Europhys. Lett.* **68**, 658 (2004).
16. N. H. Liu, *Phys. Rev. B* **55**, 3543 (1997).
17. P. Yeh, A. Yariv, and E. Murom, *J. Opt. Soc. Am.* **69**, 9 (1978).
18. Y. Xu, G. X. Ouyang, R. K. Lee, and A. Yariv, *J. Lightwave Technology* **20**, 0733 (2002).
19. Y. Fink, J. N. Winn, S. Fan, C. Chen, J. Michel, J. D. Joannopoulos, and E. L. Thomas, *Science* **282**, 1679 (1998).
20. Z. Y. Li, H. Y. Sang, L. L. Lin, and K. M. Ho, *Phys. Rev. B* **72**, 035103 (2005).
21. K. Saitoh, N. J. Florous, and M. Koshiba, *Opt. Express* **13**, 10327 (2005).

Received: 12 September 2011. Accepted: 30 November 2011.